



Sorption and migration of organophosphate flame retardants between sources and settled dust

Xiaoyu Liu ^{a,*}, Edgar Folk IV ^b

^a U.S. Environmental Protection Agency, Office of Research and Development, Center for Environmental Measurement & Modeling, Research Triangle Park, NC, 27711, USA

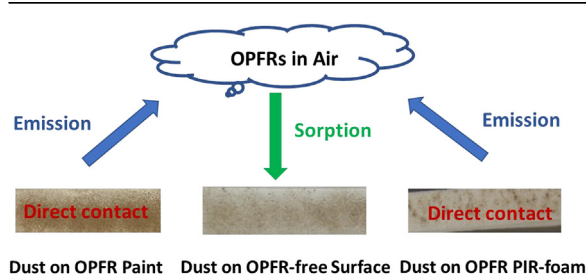
^b Jacobs, Critical Mission Solutions, EPA - Research Laboratory Support, Research Triangle Park, NC, 27711, USA



HIGHLIGHTS

- Emission, sorption, and migration of OPFRs from sources to dust were studied.
- The dust-air and dust-material partition coefficients were determined.
- The airborne particle-gas equilibrium partition coefficients were calculated.
- Dust with less organic content and smaller size tended to absorb more OPFRs.
- Volatility had less effect on dust-source partitioning than dust-air partitioning.

GRAPHICAL ABSTRACT



ARTICLE INFO

Article history:

Received 4 January 2021

Received in revised form

22 March 2021

Accepted 23 March 2021

Available online 29 March 2021

Handling Editor: Myrto Petreas

Keywords:

OPFRs

Indoor dust

Source-dust mass transfer

Dust-air partition

Small chamber

ABSTRACT

Dust serves as a strong sink for indoor pollutants, such as organophosphorus flame retardants (OPFRs). OPFRs are semivolatile chemicals that are slow in emissions but have long-term effects in indoor environments. This research studied the emission, sorption, and migration of OPFRs tris(2-chloroethyl) phosphate, tris(1-chloro-2-propyl) phosphate, and tris(1,3-dichloro-2-propyl) phosphate, from different sources to settled dust on OPFR source surfaces and OPFR-free surfaces. Four sink effect tests and six dust-source migration tests, including direct contact and sorption tests were conducted in 53 L stainless steel small chambers at 23 °C and 50% relative humidity. OPFR emission concentrations, and sorption and migration rates were determined. The dust-air and dust-material partition coefficients were estimated based on the experimental data and compared with those from the literature obtained by empirical equations. They are in the range of 1.4×10^7 to 2.6×10^8 (dimensionless) for the dust-air equilibrium partition coefficients and 2.38×10^{-3} to 0.8 (dimensionless) for the dust-material equilibrium partition coefficients. It was observed that the dust with less organic content and smaller size tended to absorb more OPFRs, but different dust did not significantly affect OPFRs emission from the same source to the chamber air. The dust-air partition favored the less volatile OPFRs in the house dust, whereas the emission from the source favored the volatile chemicals. Volatility of the chemicals had much less effect on dust-source partitioning than on dust-air partitioning. The results from this work improve our understating of the fate and mass transfer mechanisms between OPFRs sources, indoor air, surface, and dust.

Published by Elsevier Ltd.

* Corresponding author.

E-mail address: liu.xiaoyu@epa.gov (X. Liu).

1. Introduction

Many of the pollutants, including flame retardants, are semi-volatile organic compounds (SVOCs) that are released from a vast number of building materials and consumer products. Due to their adverse health effects (ATSDR, 2019), on August 13, 2015, the United States Environmental Protection Agency (US EPA) released a problem formulation for chlorinated phosphate esters used as flame retardants in furniture foams and textiles (US EPA, 2015). These chemicals are also called organophosphorus flame retardants (OPFRs), which include tris(2-chloroethyl) phosphate (TCEP, CAS# 115-96-8), tris(1-chloro-2-propyl) phosphate (TCPP, CAS# 13,674-84-5), and tris(1,3-dichloro-2-propyl) phosphate (TDCPP, CAS# 13,674-87-8). In December 2019, EPA designated TCEP as one of the twenty high-priority substances for risk evaluation under the Toxic Substances Control Act (TSCA) amended by the Frank R. Lautenberg Chemical Safety for the 21st Century Act (US EPA, 2019). On September 20, 2017, the US Consumer Product Safety Commission (CPSC) also initiated efforts to assess and issue a report on the risks to consumers' health and safety from the use of additive OPFRs in certain consumer products under the Federal Hazardous Substances Act and the Consumer Product Safety Act. (US CPSC, 2017).

OPFRs are added into manufactured products as additives for a variety of purposes (Wei et al., 2015; Lucattini et al., 2018; Moschet et al., 2018). Elevated OPFR concentrations in indoor dust have been reported by many researchers worldwide (Fan et al., 2014; Tajima et al., 2014; Langer et al., 2016). They were also measured in other microenvironments such as building material markets, private cars, floor/carpet stores, offices, bedrooms, and schools (Zhou et al., 2017; Zheng et al., 2017). Human exposure assessment by Zhou et al. (2017) concluded that dust ingestion constituted the major exposure pathway to OPFRs for toddlers and air inhalation was the major pathway for adults, while assessment by Zheng et al. (2017) indicated that the dermal contact with beddings and furniture would bring significant exposure risks for TCPP and TDCPP. Stapleton et al. (2014) also observed significant associations between OPFRs residue on children's handwipes and levels measured in house dust.

The SVOCs and dust interaction have received considerable attention as well. Most of the research has been focused on phthalate and brominated flame retardants (BFRs) (Clausen et al., 2004; Schripp et al., 2010; Rauert et al., 2014, 2015, 2016; Rauert and Harrad, 2015; Jeon et al., 2016; Qian et al., 2019; Kuribara et al., 2019; Shinohara and Uchino, 2020). Liagkouridis et al. (2017) and Tokumura et al. (2019) have examined the kinetics of TCPP and TDCPP migration from different sources to dust. Although there is a consensus on the three transport pathways, volatilization, abrasion, and migration via direct contact, between SVOCs sources and dust from these studies, little is known about their mechanisms, e.g. dust-air partitioning, dust-solid material partitioning, and particle formation. Those mass transfer mechanisms are governed by the physicochemical properties of SVOCs, such as vapor pressure (VP), octanol-air partitioning coefficients (K_{OA}), dust-air equilibrium partition coefficient (K_{da}), dust diffusion coefficients (D_d), and impacted by the properties of materials and dust and environmental conditions (Weschler and Nazaroff, 2010; Guo, 2014). These parameters can be applied to predict emissions and concentrations of SVOCs in air and dust in real environments, and thus as the required inputs for source and exposure models. Most of these data are empirical, widely variable, and inconsistent (Weschler and Nazaroff, 2010; Zhang et al., 2016; Wei et al., 2016). As a result, our knowledge of and ability to model the fate and transport of OPFRs to house dust remain limited and there is a clear need for experimental measurements and validation of those theoretically estimated data to reduce the variability and

uncertainty in the estimates of their exposures via house dust.

From 2013 to 2019, we have conducted research to develop methods and collect data for characterizing OPFRs and understanding the transport mechanisms of these chemicals between sources, air, house dust, and interior surfaces in the indoor environment. (Liu et al., 2016; Liang et al., 2018a, 2018b, 2019). The generated data reduces uncertainties and variabilities and improves confidence in rapid prediction of chemical exposure. This research paper is to report our experimental investigation of OPFRs transferred from air to settled dust and from solid sources to air and settled dust. It includes (1) settled dust on OPFR-free surfaces as the sink of constantly dosed gas-phase OPFRs; (2) OPFR emissions from source materials followed by sorption to settled dust; (3) OPFR migration from source materials to dust via direct surface contact. To the best of our knowledge, this is the first time in the literature to determine dust-air and dust-material partition coefficients of TCEP and TDCPP and dust diffusion coefficients of TCEP and TCPP when it was applicable.

2. Materials and methods

2.1. Chemicals

Certified TCEP, TCPP, and TDCPP calibration standards were purchased from AccuStandard, Inc. (New Haven, CT, USA). An isotopically labeled compound, tributyl phosphate-d27 (TBP-d27, 99.5% purity, Cambridge Isotope Laboratories, Inc., Andover, MA, USA), was used as the internal standard on the gas chromatography/mass spectrometry (GC/MS) system. Triphenyl phosphate-d15 (TPP-d15, 98% purity, Sigma-Aldrich, St. Louis, MO, USA) and tripropyl phosphate-d21 (TPP-d21, 98% purity, Cambridge Isotope Laboratories, Inc.) were used as the extraction recovery check standards (RCS).

2.2. Test materials

Three types of dust, house dust #2 (HD2), house dust #6 (HD6) and Arizona Test Dust (ATD), were used for tests. The OPFR source materials were OPFRs in polyisocyanurate rigid polyurethane foam (PIR-PUF), manufactured by ICL Industrial Products America (Gallopis Ferry, WV, USA), and in dry alkyl paint on release paper (Paul N. Gardner Company, Inc., Pampano Beach, FL, USA). The details on test material preparation are available in the Supporting Information (SI).

2.3. Sink tests

Four OPFR sorption tests on settled dust with three types of dust were conducted in a dual chamber system in the temperature-controlled incubator (Model SCN4-52, Environmental Equipment Co., Inc., Cincinnati, OH, USA) (Table S1). The 53-liter electro-polished stainless-steel chambers conform to the ASTM Standard Guide D5116-17 (ASTM, 2017). The source chamber with neat TCEP, TCPP, and TDCPP liquids from ICL in Teflon cups generated constant emissions. The other chamber that was pre-coated with the OPFRs on the wall surfaces and worked as the sink chamber was connected to the source chamber. Stainless steel "dust boats" covered with release paper were used for staging the dust particles inside the sink chamber. Fig. 1 (a, b, c) and Fig. S1 illustrate the setting of the dust sorption tests. More details are elaborated in our publication (Liu et al., 2016) and in the SI.

2.4. Migration tests

Six dust migration tests were conducted in standard 53-L

chambers placed in an incubator under different air change rates (ACRs), OPFR source materials, dust loadings, and dust types (Table S1). In these tests, 0.1–0.5 g of dust was loaded onto a PIR-PUF piece or dry alkyl paint on a release paper strip with and without OPFRs in the materials.

Test materials with dust were loaded into the chamber by opening the chamber faceplate and carefully seating the foam or paint strips containing the dust onto the floor of the chamber. After all test strips had been placed into the chamber, which included dust with OPFR materials and dust with OPFR-free materials, the chamber faceplate was closed and sealed. Inlet air flow was then reconnected, which was set to be the test start time. The chamber outlet flows were measured to verify leakage. Fig. S2 is the schematic of the dust migration test. Fig. 1d shows an example of dust-material sample layout inside the chamber.

The dust sampling took place by removing one OPFR-material strip with dust and one OPFR-free material strip with dust in a pair from the chamber after the dust was exposed to the test conditions for a specified time. The test dust was then removed from materials and solvent extracted. It is to note that we did not attempt to collect 100% of the dust from the test strips in order to minimize foam or paint into the dust sample because the chemical content in the dust was determined on a weight per weight basis (e.g., μg chemical/g dust). OPFR air concentrations inside the chamber were monitored prior to and throughout tests by collecting samples using PUF cartridge only (pre-cleaned, certified, Supelco, St. Louis, MO, USA) and polytetrafluoroethylene (PTFE) filter in the filter holder (Pall Corporation, Port Washington, NY) in front of a PUF cartridge at about 600 mL/min for 1–4 h from the

faceplate. Test durations were between 479 and 913 h.

2.5. Sample extraction and analysis

The dust, foam, release paper, and paint samples removed from the test chamber and PUF cartridges and PTFE filters were extracted and analyzed on Gas chromatography (GC)/mass spectrometry MS. The details are narrated in the SI.

2.6. Quality assurance and control

A preapproved EPA quality assurance project plan, which describes the project objectives, scientific approaches, measurement procedures, and QA/QC activities, was followed for the work. Solvent blank, extraction method blank, and field blank samples were prepared and analyzed. Recovery check standards were spiked in each of the samples to be extracted prior to extraction. Acceptance criteria for the extraction and analysis were that the recovery check standards had to be within $100 \pm 25\%$ recovery, and the precision of the duplicate samples be within $\pm 25\%$. More details are described in Liu et al. (2016).

3. Results and discussion

3.1. Test materials

Properties and scanning electron microscope images of dust and PIR-PUF are shown in Table S2 and Fig. S3. The particle size, shape, density, and organic carbon content (f_{om}) in the dust are

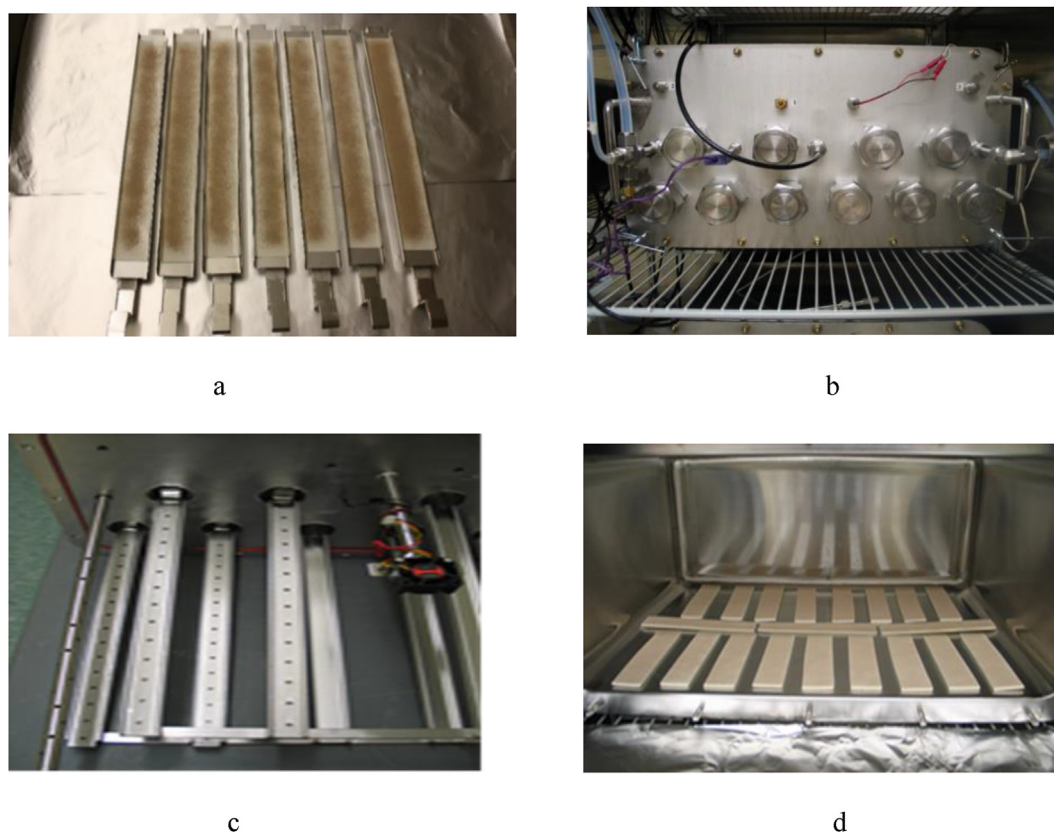


Fig. 1. Pictures showing the dust samples and test chambers for the sorption and migration tests. a: Dust on release paper, dust boats, and rods prior to placement in the sink test chamber; b: front view of the sink chamber with 10 ports used to load and remove the dust exposed to gas phase OPFRs without opening the chamber; c: the inside portion of the material chamber lid with rails to place the rods; d: dust-material sample layout inside the test chamber prior to the migration test, the strips were placed with one dust-OPFR material next to one dust-OPFR free material.

significantly different among the three types of dust. GC/MS analysis results of the total concentration of OPFRs in the OPFR-foam were in the range of 14.9%–15.9% by weight, and in the OPFR-paint it was 0.5% by weight (Table S1).

3.2. Dust as the sink of OPFRs

3.2.1. Gas-phase OPFRs

The OPFR source chamber generated constant emissions of OPFRs that were dosed continuously to the sink chamber during each test. The average concentration of TCEP, TCPP, and TDCPP ($n = 79$) with % RSD (percent relative standard deviation) measured at the outlet of the source chamber was $2.28 \mu\text{g}/\text{m}^3 \pm 26\%$, $8.40 \mu\text{g}/\text{m}^3 \pm 16\%$, and $0.78 \mu\text{g}/\text{m}^3 \pm 26\%$, respectively. The concentration of OPFR in the sink chamber air was measured at the chamber faceplate during each test and presented in Fig. S4. One advantage of this dual chamber sink test method is that only OPFR concentrations in the test chamber air were to be used for estimating partition and diffusion coefficients (Liu et al., 2016). It was observed that the concentrations in the chamber were dropped at the beginning of the test when the dust was placed inside the chamber and then gradually stabilized. No quantifiable resuspension of the settled dust was measured from the PTFE filter.

3.2.2. Sorption of OPFR on dust

SVOCs have strong adhesion to dust and the dust exists as a sink in the mass transfer process. The sink test in this study was to investigate OPFRs' interaction with dust settled on a "clean surface". Sorption of OPFRs on settled dust was a result of the dust/air partition. The dust sorption concentration (C_{ds} , $\mu\text{g}/\text{g}$) was determined experimentally and calculated by the absorbed OPFR mass in dust divided by the mass of the total sorption dust. The time-

averaged sorption rate (R_{ds} , $\mu\text{g}/\text{g}/\text{h}$) was calculated by C_{ds} divided by the exposure duration, t (h). To compare sorption behavior between different OPFRs, the normalized sorption concentration of OPFR (C_{nds} , $(\mu\text{g}/\text{g})_{\text{dust}}/(\mu\text{g}/\text{m}^3)_{\text{air}}$) and normalized sorption rate (R_{nds} , $(\mu\text{g}/\text{g}/\text{h})_{\text{dust}}/(\mu\text{g}/\text{m}^3)_{\text{air}}$) are defined as the sorption concentration and sorption rate divided by the time-averaged OPFR concentration in the chamber air during exposure period, t . The results are presented in Fig. 2 and Figs. S5 to S7.

Our results show that OPFR sorption concentrations kept increasing in all tests with TCPP being the highest and TDCPP the lowest. This was because concentrations of OPFRs in the chamber air were in the decremental order of TCPP, TCEP, and TDCPP. However, the normalized sorption concentrations and normalized sorption rates were in different orders. For house dust, HD2 and HD6, TDCPP had the highest normalized concentration and rate over time while TCEP and TCPP in both types of house dust were very close to each other, with TCEP slightly higher than TCPP. Clearly, the dust-air partition favored the less volatile OPFRs in the house dust. We observed different normalized sorption patterns for ATD, which was in the decremental order of TCPP, TDCPP, and TCEP for both ST1 and ST3. It is likely that ATD is an inorganic dust and its sorption capacity of OPFRs could be impacted by the chemical structures and properties, e.g. TDCPP contains more electronegative atoms, thus it is easier to be absorbed by inorganic dust than TCEP. Other noteworthy observation is that even after 412–888 h of exposure, the dust sorption rates of OPFRs are much slower than those at the beginning of the exposure but still far away from reaching to zero. This indicates that dust is a very strong sink.

3.2.3. Estimation of partition and diffusion coefficients

The dust-air equilibrium partition coefficient (K_{da}) and dust phase diffusion coefficient (D_d) are two of the key parameters that

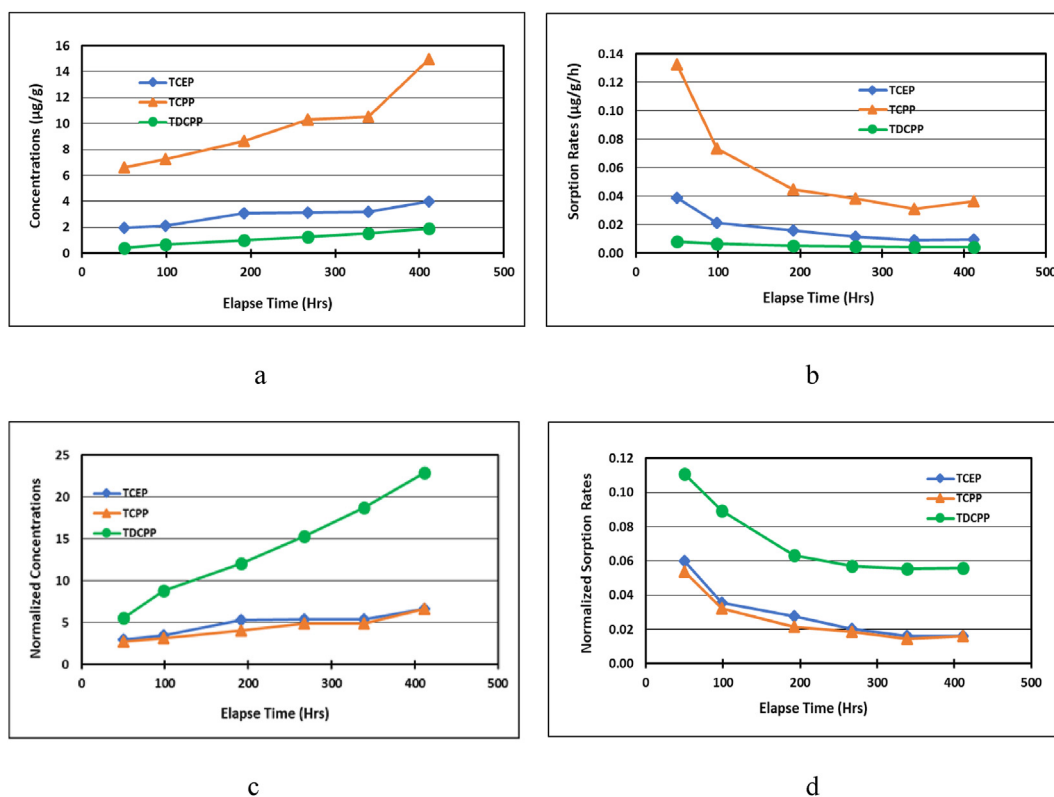


Fig. 2. OPFR (a) sorption concentrations, (b) sorption rates, (c) normalized sorption concentrations ($(\mu\text{g}/\text{g})_{\text{dust}}/(\mu\text{g}/\text{m}^3)_{\text{air}}$), and (d) normalized sorption rates $(\mu\text{g}/\text{g}/\text{h})_{\text{dust}}/(\mu\text{g}/\text{m}^3)_{\text{air}}$ in HD2 in Test ST2.

affect the interactions of air and dust. K_{da} is dimensionless, it is the ratio of OPFR concentration in the dust, C_d ($\mu\text{g}/\text{m}^3$) to its concentration in the air, C_a ($\mu\text{g}/\text{m}^3$) at equilibrium as shown in Equation (1). K_{da} can be converted to K'_{da} , which is the dust-air partition coefficient in unit of m^3/g , using Equation (2). The dust-air equilibrium partition coefficient is a measure of the sorption capacity of the dust to a specific chemical. D_d (m^2/h) characterizes the intra-particle diffusion process.

$$K_{da} = C_d / C_a \quad (1)$$

$$K'_{da} = K_{da} / (\rho \times 10^{-6}) \quad (2)$$

where ρ is the density of the dust in g/cm^3 .

In our previous study, we applied the degree of sorption saturation (DSS) model (Deng et al., 2010) to the experimentally determined sorption concentrations to estimate the material-air partition coefficient and material-phase diffusion coefficient for building materials and consumer products (Liu et al., 2014, 2016). We attempted to treat the settled dust as a solid material and use the same method to estimate K_{da} and D_d . Due to the complexity of the dust, such as size, shape, morphology, porosity, fugacity capacity, etc, and the varied values of VPs of OPFRs in the literature (Brommer et al., 2014), the method was not successful. Then, we applied iSVOC (Guo, 2013), a computer program for the dynamic modeling of the emission, transport, and sorption of SVOCs in the indoor environment to simulate the test scenarios. We input measured data, such as test environmental conditions, dust properties, and concentrations of OPFRs and estimated parameters such as K_{da} , D_d , and gas-phase mass transfer coefficient to simulate the OPFR concentration-time profile measured in the dust and air (Table S3). The simulation results were compared with experimentally determined concentration-time profiles and then applied to roughly estimate the range of K_{da} and D_d . The value of K_{da} for TCEP and TCP in ATD was about 2×10^7 and 5×10^7 , respectively, and that of D_d for TCEP and TCP in ATD was about 2×10^{-14} and 3×10^{-12} m^2/h , respectively. We were not able to obtain a good data fit of K_{da} and D_d for any other OPFR and dust combinations. Those concentrations of OPFRs in dust simulated using the parameters in Table S3 were much lower than those from the experimental data. It is to point out that the interactions of the dust with the release paper surface through direct contact was neglected in the iSVOC simulations. More work is underway to develop a dust sorption model based on the experimental data scenario reported.

3.3. OPFR migration from source to dust

Two types of tests were conducted simultaneously. One was dust on OPFR source materials, and the other was dust on OPFR-free materials. Three OPFR mass transfer processes occurred under the test conditions – emissions from sources covered with dust, migration from source to dust via direct contact, and sorption from air into dust. The data from dust on OPFR-free materials enabled us to investigate dust sorption from another perspective other than the sink tests reported above. The tests compared different types of dust, materials, dust loadings, and ACRs. OPFR concentrations in the original source materials were determined by solvent extraction (Table S1). Due to very low concentrations of source OPFRs in the PIR-PUF in the first test (MT1), most of the experimental data was below our quantification limits and thus not reported in this paper.

3.3.1. OPFR emissions from source materials

The OPFR concentrations in the chamber air were measured by

PTFE filter-PUF cartridge and PUF cartridge only sampling followed by solvent extraction. Since only zero air was introduced to the chamber and the ACRs were not greater than 1 h^{-1} for all tests, it is assumed that the chamber air was particle-free. The PTFE filter data also demonstrated that there was no quantifiable resuspension of the settled dust. The OPFR emissions from PIR-PUF were very low (below the lowest calibration concentrations, but above the instrument detection limits) and their emissions from dry alkyl paint were much higher even though the OPFR contents in the PIF-PUF was 15%, whereas in the paint was 0.5% (Fig. S8). This elucidates that the OPFR emissions from materials were dependent upon how chemicals were infused into the materials. The emission concentrations initially increased, became stable, and then gradually decreased. The reason was that during the test, the emission sources were reduced by being taken out at sampling intervals. Note that the chamber for the migration test was not pre-coated with OPFRs on the chamber wall. There is a potential possibility that the wall acts as another sink of OPFRs, but it should not be significant in this circumstance according to the data shown in Fig. S8. The emission concentrations in all tests were in the decrement order of TCP, TCEP, and TDCPP, which are in the same order as their volatility, even though their concentrations in the sources were in the reverse order. The emissions from the source favored volatile chemicals.

3.3.2. OPFR migration via direct contact

The migration concentration (C_{dm} , $\mu\text{g}/\text{g}$) at the exposure time t is the OPFR concentration in settled dust as a result of direct contact with a source. The experimentally determined migration concentrations for OPFRs are presented in Fig. 3 and Figs. S9 to S12. As shown in the figures, when the dust was in direct contact with a primary source, OPFRs migrated into the dust via dust-material partition at a much faster rate than the OPFR emissions from the sources due to the dust-air partition. Mass transfer through direct contact is highly effective. For all tests, TDCPP had the highest migration concentrations, while TCEP and TCP were close to each other with TCEP being slightly higher. This corresponded to the %wt value of individual OPFR in the sources. The migration concentration initially increased, kept relatively stable for MT2 and MT6, and then decreased after 400 h for MT3, MT4, and MT5. The data implies that there were two dynamic processes undergoing – OPFRs migration from the source material to dust and then emission to the air from dust. A plausible explanation for the concentration variation may be that part of OPFRs that had accumulated in the dust was re-emitted because of the decrease in the concentration in the air due to the removal of the source materials. This is more apparent when the original air emission concentrations were low in the chamber. This “escape” phenomenon has been observed by other studies (Clausen et al., 2004).

If we assumed that the OPFR concentration change in the source material was negligible during the tests and normalize migration concentration with the OPFR concentration ($\mu\text{g}/\text{g}$) in the source (C_{ndm} , $C_{dm}(\mu\text{g}/\text{g})_{\text{dust}}/C_s(\mu\text{g}/\text{g})_{\text{source}}$), TCP tended to have the highest normalized migration concentration and TDCPP had the lowest in MT2 and MT3 at 1 h^{-1} ACR. The effect of the VP of the chemicals on the normalized concentration in MT4 and MT5 was relatively small, where ACRs were lower.

Similarly, we defined the time-averaged migration rate (R_{dm} , $\mu\text{g}/\text{g}/\text{h}$) as the experimentally determined migration concentration divided by the exposure time and the normalized dust migration rate (R_{ndm} , $(\mu\text{g}/\text{g}/\text{h})_{\text{dust}}/(\mu\text{g}/\text{g})_{\text{source}}$) as R_{dm} divided by the OPFR concentration in the source. Both migration rates and normalized migration rates decreased over time. The normalized migration rates for different OPFRs had similar values, indicating that the volatility of the chemicals had much less effect on dust-source

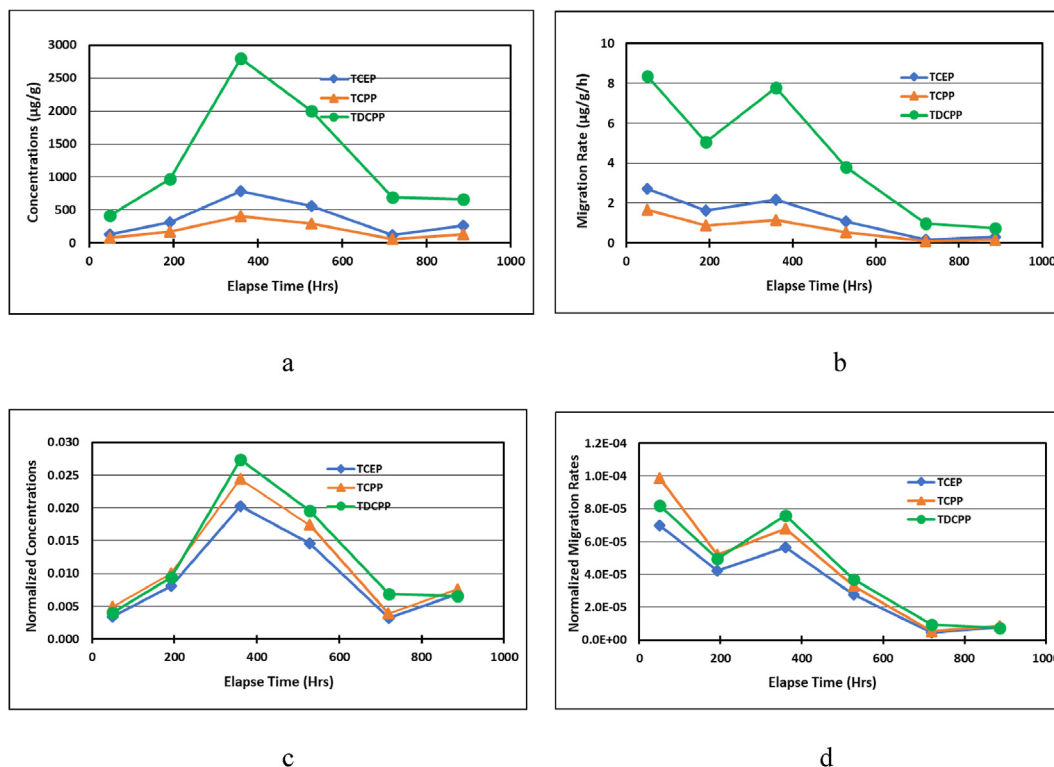


Fig. 3. OPFR (a) migration concentrations, (b) migration rates, (c) normalized migration concentrations $((\mu\text{g/g})_{\text{dust}}/(\mu\text{g/g})_{\text{source}})$, (d), normalized migration rates $(\mu\text{g/g/h})_{\text{dust}}/(\mu\text{g/g})_{\text{source}}$ in HD2 in Test MT4.

Table 1 Comparison of K'_{da} and K_{pa} values in the literature with this study^a.

Chemical	log K_{OA}	K'_{da} (m^3/g)	K_{da} (dimensionless)	K_{pa} (m^3/g)	Reference
TCEP	7.6	8.5	8.0×10^6	70.6	Zhang et al. (2016) (EPI Suite value)
	7.0	2.1	2.0×10^6	17.7	Zhang et al. (2016) (SPARC value)
	8.9	169.4	1.6×10^8	1.4×10^3	Zhang et al. (2016) (Absolv value)
	8.0 ^b	22.6	2.1×10^7	188.3	EC (2009)
		85.5	6.3×10^7	711.0	This study – ATD on PIR foam
		20.75	2.0×10^7	172.6	This study – Average of HD2 on PIR foam (n = 3)
		5.21	4.9×10^6	43.3	This study – HD2 on dry alkyl paint
TCPP	8.5	67.4	6.3×10^7	561.0	Zhang et al. (2016) (EPI Suite value)
	7.6	8.5	8.0×10^6	70.6	Zhang et al. (2016) (SPARC value)
	10.0	2.1×10^3	2.0×10^9	1.8×10^4	Zhang et al. (2016) (Absolv value)
	7.2 ^b	3.6	3.4×10^6	30.0	EC (2008a)
		29			Liagkouridis et al. (2017) (7-day's experimental value)
		224.4	1.6×10^8	1.9×10^3	This study – ATD on PIR foam
		14.8	1.4×10^7	122.9	This study – Average of HD2 on PIR foam (n = 3)
TDCPP		3.4	3.2×10^6	28.5	This study – HD2 on alkyl paint
	10.6	8.5×10^3	8.0×10^9	7.1×10^4	Zhang et al. (2016) (EPI Suite value)
	10.8	1.4×10^4	1.3×10^{10}	1.1×10^5	Zhang et al. (2016) (SPARC value)
	13.0	2.1×10^6	2.0×10^{12}	1.8×10^7	Zhang et al. (2016) (Absolv value)
	7.9 ^b	15.72	1.5×10^7	130.8	EC (2008b)
		13.7	1.0×10^7	114.1	This study – ATD on PIR foam
		273.8	2.6×10^8	2.3×10^3	This study – Average of HD2 on PIR foam (n = 3)
	42.8	4.0×10^7	355.8	This study – HD2 on alkyl paint	

^a Unless otherwise noted, for all literature data in this table, log K_{OA} data was from the cited literature; K'_{da} was calculated using Equation (4) with HD2 data $f_{om} = 0.2$, $\rho = 0.938 \text{ g/m}^3$; K_{da} was calculated using Equation (2); K_{pa} was calculated using Equation (6).
^b K_{OA} was calculated using Equation (5) at $T = 25 \text{ }^\circ\text{C}$ (298 K) with Kow and H data from European Union risk assessment reports.

partitioning than on dust-air partitioning. This hypothesis is supported by previous studies (Clausen et al., 2004; Raurert et al., 2016; Sukiene et al., 2017). Tokumura et al. (2019), who compared the direct migration rates of TDCPP from polyester curtains to indoor dust, concluded that VP was not the predominant physicochemical property for the direct migration pathway, and that $K_{ow}/\log K_{ow}$ (dimensionless) played a role with higher log K_{ow} having higher

affinity for hydrophobic materials such as indoor dust.

3.3.3. OPFR sorption to settled dust

The settled dust on OPFR-free materials absorbed the gas-phase OPFRs that emitted from the OPFR source materials covered with dust in the chamber. These sorption concentrations were much lower than the migration concentrations via direct contact for all

tests. The results are shown in Fig. S13.

Since the migration tests lasted about 900 h, and the air concentrations in the chamber and in the settled dust on OPFR-free materials tended to be stabilized, we calculated K_{da} and K'_{da} using Equations (1) and (2) and listed their results in Table 1. These data are estimated values because (1) it was assumed that the test conditions were equilibrium at the end, but in reality, it may have not been reached yet; (2) sink effect of the chamber wall was not taken into account; (3) due to the low emissions of OPFR in the migration tests, the values of C_a and C_d in the calculation of K_{da} from migration tests may have caused some experimental errors. We could not tell what the "true value" is without further study, but the significance of this work is that it provided a particle range of K_{da} and K'_{da} for different types of indoor dust on different source materials through experimental data rather than theoretical calculations that treat all the materials the same.

3.3.4. Estimation of the dust/source partition coefficients

The amount of OPFRs transferred from the source materials to the dust depends on dust-source partition, diffusivities, and distributions of OPFRs in dust and source materials. The dust-source partition coefficient (K_{dm}) at equilibrium can be calculated by the ratio of equilibrium concentrations in dust vs. source. Our test results show that the migration concentrations of OPFRs in dust became stabilized at the end of test. Thus, we calculated K_{dm} , between dust and source material, which is dimensionless, using Equation (3).

$$K_{dm} = C'_d / C_m \quad (3)$$

where C'_d is the OPFR concentration in dust in equilibrium with source material, $\mu\text{g/g}$, and C_m is the OPFR concentration in the source material in equilibrium with dust, $\mu\text{g/g}$. Their estimated values are shown in Table 2. It was observed from the Table that the mass transfer strength of the three OPFRs from the PIR-PUF and the alkyl paint to the dust were very close to each other from the same source material. The data evidenced that the migration due to dust-source partitioning was not significantly affected by the volatilities of the chemicals.

3.3.5. Effect of dust loading

The effect of dust loading on migration from source to dust and sorption from air to dust were evaluated in three tests (MT2, MT3, and MT6). Dust loading at four levels between 0.1 and 0.5 g per material strip were applied and exposed to the source material and the OPFRs in the chamber air. They were all taken out within 5 min at the end of each test. The results of these tests are displayed in Fig. S15. The migration concentrations and rates were not notably affected by the HD2 dust loadings but positively decreased with increasing ATD dust amount. The sorption concentrations and rates of OPFRs decreased when the ATD and HD2 dust loadings were increased in PIR-PUF tests. However, the effect of HD2 dust loading

Table 2
Calculated dust-material partition coefficients (K_{dm}) at the end of migration tests^a.

Test ID	Dust	Material	K_{dm} (dimensionless)		
			TCEP	TCPP	TDCPP
MT2	ATD	PIR-PUF	1.34×10^{-2}	1.80×10^{-2}	3.51×10^{-3}
MT3	HD2	PIR-PUF	8.55×10^{-3}	9.31×10^{-3}	8.77×10^{-3}
MT4	HD2	PIR-PUF	6.84×10^{-3}	7.63×10^{-3}	6.53×10^{-3}
MT5	HD2	PIR-PUF	2.59×10^{-3}	2.69×10^{-3}	2.38×10^{-3}
MT6	HD2	Alkyl paint	0.80	0.55	0.39

^a MT1 is not reported because most of the experimental data was below our quantification limits.

on OPFR sorption was not significant when the dust was on painted surfaces. It is possible that the different amount of dust loaded on the surface materials changed the distribution, thickness of the dust layer and surface area more for ATD than for house dust because house dust has much larger sized particles. The finding from ATD tests that increment of dust loading decreased the migration rate is consistent with Shinohara and Uchino's work (2020) that the transfer rates per dust weight increased with the decrease of the dust weight on the polyvinyl chloride sheet. It is explained by Liangkouridis et al. (2017) that an excess amount of dust might have resulted in a lower surface available for chemical partitioning. However, our HD2 test data does not support this hypothesis. The different test conditions of this study and other factors, such as dust properties, might also contribute to the different kinetics.

3.3.6. Effect of air change rate

The impact of ventilation on OPFR emission, and migration was investigated under 0.25 (MT5), 0.5 (MT4), and 1 (MT3) h^{-1} ACRs in the migration tests. As mentioned before, the measured air emission concentrations from the OPFR PIR-PUF covered with HD2 were all low under the test conditions. However, we still observed the trends that the air concentrations were considerably higher at 0.25 and 0.5 h^{-1} than those at 1 h^{-1} and that the concentrations at 0.25 and 0.5 h^{-1} were comparable to each other. The impacts of ACR on migration concentration and migration rate are presented in Fig. S14. The data shows that the migration concentrations and rates for all three OPFRs are consistently lower when the ACR was higher, especially at 1 h^{-1} . These results revealed the role of ventilation in the mass transfer between OPFR, dust, air, and material surfaces.

3.3.7. Effect of source material

HD2 was loaded on PIR-PUF (MT3) and dry alkyl paint (MT6) for this investigation. The same test procedures were followed in both tests to compare the emission, migration, and sorption results. As mentioned before, because of the different conditions of the materials, e.g. porosity and roughness, surface finishing, and the way OPFRs were infused into the materials, OPFRs in dry alkyl paint had much higher emission, migration concentration, and migration rates, whereas the sorption concentration and sorption rates were comparable for both materials. This implies that the sorption process occurred at the dust surface, not the material surfaces during the exposure time in those tests.

3.3.8. Effect of different dust

The comparison of different dusts was conducted through MT2 and MT3 tests as well as in the sink tests. The emission concentrations of OPFRs from the same source covered with ATD and HD2 dust respectively, were close to each other, suggesting that the dust type did not significantly affect the emission of OPFRs to the chamber air. This is consistent with the recent report by Qian et al. (2019) for BFRs.

In general, ATD absorbs more gas-phase OPFRs at faster rates than house dust. In the sink tests, the normalized sorption concentrations and sorption rates of OPFRs in dust were in the incremental order HD2, HD6, and ATD, which was in the reverse order of the wt% value of organic contents in the dust. The sorption rates of OPFRs in ATD dust kept relatively stable but those in HD2 and HD6 decreased rapidly before 200 h then slowed down thereafter.

In the dust migration tests, the migration concentrations and normalized migration concentrations were almost three times higher for ATD than for HD2, and the sorption concentrations and normalized sorption concentrations were about two times higher for ATD than for HD2. The fact that enrichment of OPFRs on ATD

compared to HD2 was consistent with the results from our sink tests. In contrast to the concentrations, the migration rates, normalized migration rates, sorption rates and normalized sorption rates are comparable to each other between ATD and HD2 with similar trends – migration rates decreased over time for both ATD and HD2 whereas sorption rates decreased for house dust but kept relatively stable for ATD.

As shown in Table S1, ATD had almost 15 to 19 times smaller particle size and two times more surface area than HD2 and HD6. These features usually make pollutant transport easier. Under the same exposure conditions, ATD can take up more OPFRs than house dust and the difference is greater for dust-source partitioning than for dust-air partitioning. It should also be mentioned that ATD had much less organic content than house dust. In general, organic compounds are more lipophilic than most inorganic compounds. These results suggested that two factors, the particle size and organic content, could offset each other. Our results are consistent with those from Rauert et al. (2016) who studied direct contact between dust and (HBCD)-treated fabrics and concluded that HBCD transfer was not dominated solely by dust organic content. However, Schripp et al. (2010) reported that higher di-*n*-butyl phthalate concentrations were detected in dust and soil than sand, which had lower organic content. Another alternative explanation given by Liagkouridis et al. (2017) is that the presence of dust particles on the product surface can increase surface “roughness” and thus decrease the “resistance” for product to air diffusive transfer. Recently, through their flame retardants’ studies He et al. (2018) and Qian et al. (2019) concluded that for flame retardants with $\log K_{ow} < 4$, the property all three tested OPFRs possess, their accumulation in dust was mainly controlled by dust surface areas instead of organic carbon contents.

3.4. Comparison with literature data

The research results from our present study were consistent with literature in that direct transfer between settled dust and source material surface is an important and effective pathway for pollutant mass transfer. More detailed discussions were presented above.

In the literature, empirical Equation (4) was frequently used to estimate K'_{da} when measured data was not available (Weschler and Nazaroff, 2010).

$$K'_{da} = f_{om} \times K_{OA} / \rho \quad (4)$$

where f_{om} is the fraction of organic matter of settled dust. There are wide variations in the estimated values of K_{OA} in the literature. For comparison, we used K_{OA} values estimated using EPISuite, SPARC, and Absolv in the literature (Zhang et al., 2016) and calculated value using Equation (5) (Bennett and Furtaw, 2004):

$$K_{OA} = K_{OW} \times RT/H \quad (5)$$

where H is the Henry's law constant ($\text{Pa} \cdot \text{m}^3/\text{mol}$), R is the ideal gas constant ($8.314 \text{ Pa} \cdot \text{m}^3/\text{mol} \cdot \text{K}$), and T is the temperature (K). In the calculation, K_{ow} and H were obtained from European Union risk assessment reports (2009, 20,081, 2008b). Equation (6) from literature (Wei et al., 2016) was used to estimate the airborne particle-gas equilibrium partition coefficients, K_{pa} (m^3/g).

$$K_{pa} = 8.32 \times K'_{da} \quad (6)$$

The calculated values and our experimental data are compared and summarized in Table 1. It is worth mention that the empirical calculations utilized the HD2 experimental data, $f_{om} = 0.2$ and

$\rho = 0.938 \text{ g}/\text{m}^3$. From Table 1, the dust-air and airborne particle-air equilibrium partition coefficients obtained from experimental data fall into their empirically estimated range for all three OPFRs. These data are somewhat comparable to each other, generally within 1–2 orders of magnitude. Due to the uncertainties in the empirical calculations and potential measurement problems, e.g. it is possible that equilibrium had not been attained, it is difficult to know at this point which values are more accurate. Nevertheless, these data provide the available ranges of K_{da} and K_{pa} experimentally as opposed to theoretically. The experimental data reported from this study is the first in the literature.

4. Conclusions

In this work, we conducted carefully designed chamber experiments and investigated the underlying mechanisms of emission, sorption, and migration of OPFRs between sources and settled dust in detail. Our results should enlighten the correlations between OPFR concentrations in settled dust, surface materials, and air. We provided strong evidence that OPFRs migrate effectively from the source material to the dust covered on the material. The emission from the source material favors the volatile OPFRs and the sorption by the dust favors the less volatile chemicals. Based on our data, factors such as the type of dust, dust loading, source material, and ventilation affect the OPFR mass transfer process. The values of D_d , K_{da} , K'_{da} , K_{dm} , and K_{pa} presented in this study, though rough estimates, were informed by measured data, and compared with the literature data obtained from empirical calculations. Our next step is to develop mass transfer models to more accurately quantify the diffusion coefficients and partition coefficient. Our goal is to further characterize the variability and reduce uncertainties of the data and improve confidence in the estimations of OPFRs exposures through dust.

Declaration of competing interest

The authors declare that they have no known competing financial interests or personal relationships that could have appeared to influence the work reported in this paper.

Acknowledgements

We thank ICL Industrial Products America, Inc. For providing the PIR-PUF foam and OPFR chemicals, U.S. EPA's in-house contractors, Jacobs' former employees, Matthew R. Allen and Christopher Fuller, and Nancy F. Roach who worked for Arcadis US for conducting the chamber tests, Bakul Patel from U.S. EPA Center for Environmental Measurement & Modeling for conducting OC/EC analysis of the dust, Cathy Fehrenbacher and Eva Wong from EPA Office of Pollution Prevention and Toxics (OPPT) and EPA OPPT former employee Charles Bevington for discussion and consultation.

Appendix A. Supplementary data

Supplementary data to this article can be found online at <https://doi.org/10.1016/j.chemosphere.2021.130415>.

Disclaimer

The views expressed in this article are those of the authors and do not necessarily represent the views or policies of the U.S. EPA. Mention of trade names or commercial products does not constitute endorsement or recommendation for use by the U.S. EPA. The authors declare no competing financial interest.

Credit author statement

Xiaoyu Liu: Conceptualization, Methodology, Data curation, Formal analysis, Funding acquisition, Project administration, Writing – original draft. Edgar Folk IV: Investigation, Writing – Reviewing & Editing

References

- ASTM D5116-17, 2017. Standard Guide for Small-Scale Environmental Chamber Determinations of Organic Emissions from Indoor Materials/products. ASTM International, West Conshohocken, PA. <https://compass.astm.org/CUSTOMERS/login.html>.
- ATSDR, 2019. U.S. Department of Health and Human Services, Agency for Toxic Substances and Disease Registry. Toxicology profile for phosphate ester flame retardants. <https://www.atsdr.cdc.gov/ToxProfiles/tp.asp?id=1119&tid=239>.
- Bennett, D.H., Furtaw Jr., E.J., 2004. Fugacity-based indoor residential pesticide fate model. *Environ. Sci. Technol.* 38, 2142–2152. <https://doi.org/10.1021/es034287m>.
- Brommer, S., Jantunen, L.M., Bidleman, T.F., Harrad, S., Diamond, M.L., 2014. Determination of vapor pressures for organophosphate esters. *J. Chem. Eng. Data* 59 (5), 1441–1447. <https://doi.org/10.1021/je401026a>.
- Clausen, P.A., Hansen, V., Gunnarsen, L., Afshari, A., Wolkoff, P., 2004. Emission of di-2-ethylhexyl phthalate from PVC flooring into air and uptake in dust: emission and sorption experiments in FLEC and CLIMPAQ. *Environ. Sci. Technol.* 38, 2531–2537. <https://doi.org/10.1021/es0347944>.
- Deng, Q., Yang, X., Zhang, J.S., 2010. New indices to evaluate volatile organic compound sorption capacity of building materials (RP-1321). *HVAC R Res.* 16, 95–105. <https://www.tandfonline.com/doi/abs/10.1080/10789669.2010.10390894>.
- European Communities (EC), 2009. European Union Risk Assessment Report, TRIS (2-CHLOROETHYL) PHOSPHATE, TCEP, CAS-No. 115-96-8. <https://echa.europa.eu/documents/10162/26663989d-1795-44a1-8f50-153a81133258>.
- European Communities (EC), 2008a. European Union Risk Assessment Report, TRIS(2-CHLORO-1-METHYLETHYL) PHOSPHATE, (TCPP). CAS No: 13674-84-5. <https://echa.europa.eu/documents/10162/8a6e5c7c-15d6-4e80-b083-0cca700c32d3>.
- European Communities (EC), 2008b. European Union Risk Assessment Report, TRIS [2-CHLORO-1(CHLOROMETHYL)ETHYL] PHOSPHATE (TDCP). CAS No: 13674-87-8. https://echa.europa.eu/documents/10162/6434698/orats_final_rar_tris2-chloro-1-chloromethyleth_en.pdf.
- Fan, X., Kubwabo, C., Rasmussen, P.E., Wu, F., 2014. Simultaneous determination of thirteen organophosphate esters in settled indoor house dust and a comparison between two sampling techniques. *Sci. Total Environ.* 491–492, 80–86. <https://doi.org/10.1016/j.scitotenv.2013.12.127>.
- Guo, Z., 2014. A framework for modelling non-steady-state concentrations of semivolatile organic compounds indoors – II. Interactions with particulate matter. *Indoor Built Environ.* 23, 26–43. <https://doi.org/10.1177/1420326X13496802>.
- Guo, Z., 2013. I-SVOC – A Simulation Program for Indoor SVOCs. US Environmental Protection Agency, Cincinnati, OH. EPA/600/C-13/290, Version 1.0. <https://www.epa.gov/chemical-research/indoor-semi-volatile-organic-compounds-i-svoc-version-1.0>.
- He, R., Li, Y., Xiang, P., Li, C., Cui, X., Ma, L.Q., 2018. Impact of particle size on distribution and human exposure of flame retardants in indoor dust. *Environ. Res.* 162, 166–172. <https://doi.org/10.1016/j.envres.2017.12.014>.
- Jeon, S., Kim, K., Choi, K., 2016. Migration of DEHP and DINP into dust from PVC flooring products at different surface temperature. *Sci. Total Environ.* 547, 441–446. <https://doi.org/10.1016/j.scitotenv.2015.12.135>.
- Kuribara, I., Kajiwara, N., Sakurai, T., Kuramochi, H., Motoki, T., Suzuki, G., Wada, T., Sakai, S., Takigami, H., 2019. Time series of hexabromocyclododecane transfers from flame-retarded curtains to attached dust. *Sci. Total Environ.* 696, 133957. <https://doi.org/10.1016/j.scitotenv.2019.133957>.
- Langer, S., Fredricsson, M., Weschler, C.J., Bekö, G., Strandberg, B., Remberger, M., Toftum, J., Clausen, G., 2016. Organophosphate esters in dust samples collected from Danish homes and daycare centers. *Chemosphere* 154, 559–566. <https://doi.org/10.1016/j.chemosphere.2016.04.016>.
- Liang, Y., Liu, X., Allen, M.R., 2018a. Measuring and modeling surface sorption dynamics of organophosphate flame retardants on impervious surfaces. *Chemosphere* 193, 754–762. <https://doi.org/10.1016/j.chemosphere.2017.11.080>.
- Liang, Y., Liu, X., Allen, M.R., 2018b. Measurements of parameters controlling the emissions of organophosphate flame retardants in indoor environments. *Environ. Sci. Technol.* 52, 5821–5829. <https://doi.org/10.1021/acs.est.8b00224>.
- Liang, Y., Liu, X., Allen, M.R., 2019. The influence of temperature on the emissions of organophosphate ester flame retardants from polyisocyanurate foam: measurement and modeling. *Chemosphere* 233, 347–354. <https://doi.org/10.1016/j.chemosphere.2019.05.289>.
- Liagkouridis, I., Lazarov, B., Giovanoulis, G., Cousins, I.T., 2017. Mass transfer of an organophosphate flame retardant between product source and dust in direct contact. *Emerging Contaminants* 3, 115–120. <https://doi.org/10.1016/j.emcon.2017.09.002>.
- Liu, X., Guo, Z., Roache, R.F., 2014. Experimental method development for estimating solid-phase diffusion coefficients and material/air partition coefficients of SVOCs. *Atmos. Environ.* 89, 76–84. <https://doi.org/10.1016/j.atmosenv.2014.02.021>.
- Liu, X., Roache, N.F., Allen, M.R., 2016. Characterization of organophosphorus flame retardants' sorption on building materials and consumer products. *Atmos. Environ.* 140, 333–341. <https://doi.org/10.1016/j.atmosenv.2016.06.019>.
- Lucattini, L., Poma, G., Covaci, A., de Boer, J., Lamoree, M.H., Leonards, P.E.G., 2018. A review of semi-volatile organic compounds (SVOCs) in the indoor environment: occurrence in consumer products, indoor air and dust. *Chemosphere* 201, 466–482. <https://doi.org/10.1016/j.chemosphere.2018.02.161>.
- Moschet, C., Anumol, T., Lew, B.M., Bennett, D.H., Young, T.M., 2018. Household dust as a repository of chemical accumulation: new insights from a comprehensive high-resolution mass spectrometric study. *Environ. Sci. Technol.* 52, 2878–2887. <https://doi.org/10.1021/acs.est.7b05767>.
- Qian, Z., Xu, Y., Zheng, C., Zhang, A., Sun, J., 2019. Enhanced emissions of brominated flame retardants from indoor sources by direct contact with dust. *Environ. Monit. Assess.* 191, 170. <https://link.springer.com/article/10.1007/s10661-019-7303-9>.
- Rauert, C., Harrad, S., 2015. Mass transfer of PBDEs from plastic TV casing to indoor dust via three migration pathways – a test chamber investigation. *Sci. Total Environ.* 536, 568–574. <https://doi.org/10.1016/j.scitotenv.2015.07.050>.
- Rauert, C., Harrad, S., Stranger, M., Lazarov, B., 2015. Test chamber investigation of the volatilization from source materials of brominated flame retardants and their subsequent deposition to indoor dust. *Indoor Air* 25, 393–404. <https://doi.org/10.1111/ina.12151>.
- Rauert, C., Harrada, S., Suzuki, G., Takigami, H., Uchida, N., Takatab, K., 2014. Test chamber and forensic microscopy investigation of the transfer of brominated flame retardants into indoor dust via abrasion of source materials. *Sci. Total Environ.* 493, 639–648. <https://doi.org/10.1016/j.scitotenv.2014.06.029>.
- Rauert, C., Kuribara, I., Kataoka, T., Wada, T., Kajiwara, N., Suzuki, G., Takigami, H., Harrad, S., 2016. Direct contact between dust and HBCD-treated fabrics is an important pathway of source-to-dust transfer. *Sci. Total Environ.* 545–546, 77–83. <https://doi.org/10.1016/j.scitotenv.2015.12.054>.
- Schripp, T., Fauck, C., Salthammer, T., 2010. Chamber studies on mass-transfer of di(2-ethylhexyl)phthalate (DEHP) and di-n-butylphthalate (DnBP) from emission sources into house dust. *Atmos. Environ.* 44, 2840–2845. <https://doi.org/10.1016/j.atmosenv.2010.04.054>.
- Shinohara, N., Uchino, K., 2020. Diethylhexyl phthalate (DEHP) emission to indoor air and transfer to house dust from a PVC sheet. *Sci. Total Environ.* 711, 134573. <https://doi.org/10.1016/j.scitotenv.2019.134573>.
- Stapleton, H.M., Misenheimer, J., Hoffman, K., Webster, T.F., 2014. Flame retardant associations between children's handwipes and house dust. *Chemosphere* 116, 54–60. <https://doi.org/10.1016/j.chemosphere.2013.12.100>.
- Sukiene, V., von Goetz, N., Gerecke, A.C., Bakker, M.I., Delmaar, C.J.E., Hungerbühler, K., 2017. Direct and air-mediated transfer of labeled SVOCs from indoor sources to dust. *Environ. Sci. Technol.* 51, 3269–3277. <https://doi.org/10.1021/acs.est.6b06051>.
- Tajima, S., Araki, A., Kawai, T., Tsuboi, T., Ait Bamai, Y., Yoshioka, E., Kanazawa, A., Cong, S., Kishi, R., 2014. Detection and intake assessment of organophosphate flame retardants in house dust in Japanese dwellings. *Sci. Total Environ.* 478, 190–199. <https://doi.org/10.1016/j.scitotenv.2013.12.121>.
- Tokumura, M., Ogo, S., Kume, K., Muramatsu, K., Wang, Q., Miyake, Y., Amagai, T., Makino, M., 2019. Comparison of rates of direct and indirect migration of phosphorus flame retardants from flame-retardant-treated polyester curtains to indoor dust. *Ecotoxicol. Environ. Saf.* 169, 464–469. <https://doi.org/10.1016/j.ecoenv.2018.11.052>.
- US CPSC, 2017. Guidance for Hazardous Additive, Non-polymeric Organohalogen Flame Retardants in Certain Consumer Products. <https://www.cpsc.gov/Business-Manufacturing/Business-Education/Business-Guidance/flame-retardants>.
- US EPA, 2015. Assessments Conducted on TSCA Work Plan Chemicals Prior to June 22, 2016. In: <https://www.epa.gov/assessing-and-managing-chemicals-under-tsca/assessments-conducted-tsca-work-plan-chemicals-prior#process>.
- US EPA, 2019. EPA Finalizes List of Next 20 Chemicals to Undergo Risk Evaluation under TSCA. <https://www.epa.gov/newsreleases/epa-finalizes-list-next-20-chemicals-undergo-risk-evaluation-under-tsca>.
- Wei, G., Lia, D., Zhuo, M., Liao, Y., Xie, Z., Guo, T., Li, J., Zhang, S., Liang, Z., 2015. Organophosphorus flame retardants and plasticizers: sources, occurrence, toxicity and human exposure. *Environ. Pollut.* 196, 29–46. <https://doi.org/10.1016/j.envpol.2014.09.012>.
- Wei, W., Mandin, C., Blanchard, O., Mercier, F., Pelletier, M., Le Bot, B., Glorennec, P., Ramalho, O., 2016. Distributions of the particle/gas and dust/gas partition coefficients for seventy-two semi-volatile organic compounds in indoor environment. *Chemosphere* 153, 212–219. <https://doi.org/10.1016/j.chemosphere.2016.03.007>.
- Weschler, C.J., Nazaroff, W.W., 2010. SVOC partitioning between the gas phase and settled dust indoors. *Atmos. Environ.* 44, 3609–3620. <https://doi.org/10.1016/j.atmosenv.2010.06.029>.
- Zhang, X., Sührling, R., Serodio, D., Bonnell, M., Sundin, N., Diamond, M.L., 2016. Novel flame retardants: estimating the physical chemical properties and environmental fate of 94 halogenated and organophosphate PBDE replacements. *Chemosphere* 2401–2408. <https://doi.org/10.1016/j.chemosphere.2015.11.017>.

Zheng, X., Qiao, L., Covaci, A., Sun, X., Guo, H., Zheng, J., Luo, X., Xie, Q., Mai, B., 2017. Brominated and phosphate flame retardants (FRs) in indoor dust from different microenvironments: implications for human exposure via dust ingestion and dermal contact. *Chemosphere* 184, 185–191. <https://doi.org/10.1016/j.chemosphere.2017.05.167>.

Zhou, L., Hiltcher, M., Püttmann, W., 2017. Occurrence and human exposure assessment of organophosphate flame retardants in indoor dust from various microenvironments of the Rhine/Main Region, Germany. *Indoor Air* 27 (6). <https://doi.org/10.1111/ina.12397>, 1113–1127.